ACS APPLIED ENERGY MATERIALS

Article

Cite This: ACS Appl. Energy Mater. 2019, 2, 8153−8162

www.acsaem.org

Double-Shelled Co_3O_4/C Nanocages Enabling Polysulfides Adsorption for High-Performance Lithium−Sulfur Batteries

Lei Zhou,[†,‡] Hao Li,[§] Xiaochao Wu,[‡,∥] Yue Zhang,[†] Dmitri L. Danilov,[†,‡] Rüdiger-A. Eichel,[‡,∥] and Peter H. L. Notten*[,†,‡,⊥]

[†]Eindhoven University of Technology, P.O. Box 513, 5600 MB Eindhoven, The Netherlands

[‡]Institute of Energy and Climate Research, Fundamental Electrochemistry (IEK-9), Forschungszentrum Jülich, D-52425 Jülich, Germany

[§]Key Laboratory of Optoelectronic Devices and Systems of Ministry of Education and Guangdong Province, College of Optoelectronic Engineering, Shenzhen University, Shenzhen 518060, China

[∥]Institute of Physical Chemistry, RWTH Aachen University, D-52074 Aachen, Germany

[⊥]Centre for Clean Energy Technology, University of Technology Sydney, Broadway, Sydney, New South Wales 2007, Australia

Supporting Information

ABSTRACT: Rechargeable lithium−sulfur (Li−S) batteries, which originate from the merits of extraordinary theoretical specific energy density, abundant resources, and eco-friendly character, have received ever-growing attention. However, their practical applications are seriously hampered because of the poor conductive property of the sulfur and the discharging products, severe dissolution and migration of lithium polysulfide intermediates, and huge volumetric variation of sulfur particles upon cycling. Here, double-shelled Co_3O_4 and carbon (Co_3O_4/C) hollow nanocages as sulfur host materials are reported. The double-shelled structures can significantly boost the adsorption of soluble polysulfides and the electrical conductivity of sulfur cathodes. Consequently, the prepared S@Co_3O_4/C cathodes achieve considerable capacity enhancement and excellent rate capability, combining the durable cycling life at 1 C for 500 cycles, in which the overall capacity fading remains as low as 0.083% per cycle. Upper-plateau (Q_H) and lower-plateau (Q_L) capacities, static adsorption of polysulfides, and X-ray photoelectron spectroscopy (XPS) analyses unveil the underlying nature of the chemical interactions between polysulfide species and the sulfur host. The present results will favor the design and screening of prospective host materials to boost future Li−S batteries.

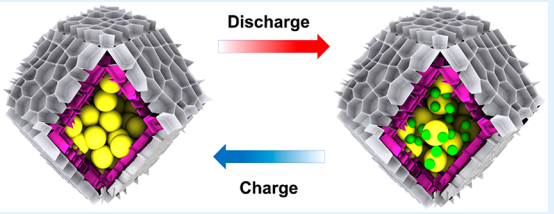

KEYWORDS: *double-shelled structure, lithium−sulfur batteries, metal oxides, polysulfides, chemical adsorption*

1. INTRODUCTION

With the depletion of traditional fossil fuels and increasing demands for consumer electronics and electric vehicles, etc., numerous scientific research studies have been conducted to exploit rechargeable batteries with high energy density.[1] Despite great success having been achieved, traditional lithium-ion batteries using lithium-containing oxides or phosphates as cathode materials (e.g., $LiCoO_2$ and $LiFePO_4$) suffer from low-density energy and capacity, impeding their applications on energy storage systems.[2] In addition, the high cost and environmental inconvenience arising from traditional cathode materials further thwart extensive use in industry. As a result, the exploration of superior and highly cost-effective energy storage technologies is now at the top of the agenda.

Lithium−sulfur (Li−S) batteries have been perceived as potential alternatives for advanced battery technologies for the next generation in terms of the theoretical specific energy density which is as high as 2600 Wh kg^{-1} stemming from a two-electron redox reaction between metallic lithium and sulfur ($2Li + S = Li_2S$), 6−7 times that of the currently commercialized lithium-ion batteries.[3−5] Furthermore, abundant resources and high biocompatibility of elemental sulfur boost the potential for commercialization of Li−S batteries. However, there are some drawbacks existing in current Li−S batteries, which severely hamper their practical applications.[6,7] One of the principal issues is that the nonconductive properties of elemental sulfur and lithium sulfide (Li_2S) incur a large battery polarization, decreasing the electrochemical utilization of sulfur. Another problem lies in the dissolution of lithium polysulfide intermediates out of the cathodes. The detrimental shuttle effect causes heavy losses of the active sulfur materials and poor Coulombic efficiency. Also, the volume variation of sulfur particles upon cycling, which pulverizes the active materials and gives rise to fast capacity degradation, still persists. Therefore, considerable efforts should be devoted to the design of efficient sulfur-encapsulating materials to overcome these conundrums, achieving superior capacity and durable cycling stability.

Received: August 20, 2019
Accepted: October 31, 2019
Published: October 31, 2019

DOI: 10.1021/acsaem.9b01621
ACS Appl. Energy Mater. 2019, 2, 8153−8162

It has been demonstrated that carbon-based materials with highly porous structures can enhance the electrical conductivity and physical adsorption of lithium polysulfides.[8] Encapsulating active sulfur species in host materials like graphene,[9−12] carbon nanotubes,[13−16] porous carbons, or conductive polymers results in an improved electrochemical performance of Li−S batteries.[17−21] However, the nonpolarity of carbon-based materials indicates the low affinity with polar lithium polysulfides, which fails to efficiently bind and anchor lithium polysulfides within the cathode. As a result, carbon-based materials alone can facilitate electron transport and electrochemical kinetics but are still unable to inhibit the loss of active sulfur species. Recently, various polar materials possessing strong chemical interactions with lithium polysulfides, including metal oxides,[22−25] metal hydroxides,[26−30] metal sulfides,[31−37] and metal−organic frameworks (MOFs),[38−42] have been employed to mitigate the dissolution and diffusion of soluble polysulfide intermediates out of the cathode. On the other hand, the rate capability is compromised due to the relatively poor electrical conductivity of many polar metallic compounds. It is therefore favorable to design electrodes which combine highly conductive carbon-based materials with polar polysulfide-anchoring materials to synergistically ensure the utilization of lithium polysulfides and facilitate fast electron transport, thus contributing to enhanced battery performance.

In this work, we propose the design and preparation of double-shelled Co_3O_4 and carbon (Co_3O_4/C) hollow nanocage structures as advanced sulfur hosts to substantially anchor polysulfide species inside the cathode, thus achieving the performance boost for Li−S batteries. The synergetic effects of double-shelled Co_3O_4/C nanocage structures are responsible for the various merits of sulfur cathodes. First, the outer carbon shells provide superior conductivity for fast electron transference, significantly accelerating the charge transfer kinetics. Also, the carbon shells can act as the block of soluble polysulfides to impede their diffusion. In addition, the inner polar Co_3O_4 shells can strongly anchor polysulfides via chemical adsorption to prevent them from diffusing to the electrolyte. Thus, the active sulfur species were well-trapped in the hollow nanocages, resulting in effective utilization of sulfur.[43,44] Finally, the double-shelled nanocage architecture with sufficient void space enables high sulfur content and mitigates large volume variation of sulfur particles upon cycling. Compared with other Co_3O_4 structures reported in sulfur cathodes, Co_3O_4/C integrated many important advantages of the strong adsorption of polysulfides, enhanced conductivity, high ability to accommodate sulfur, and effective mitigation of volume variation of sulfur particles upon cycling, providing a novel and effective strategy to fabricate advanced sulfur host materials with high performance. As expected, the above synergistic effects entail S@Co_3O_4/C cathodes with significantly enhanced specific capacity, favorable rate performance, as well as outstanding cycling life, demonstrating the superiority of double-shelled Co_3O_4/C nanocage structures.

2. EXPERIMENTAL SECTION

2.1. Synthesis of ZIF-67. Typically, cobalt nitrate hexahydrate (0.5 g) and 2-methylimidazole (0.8 g) were dissolved in methanol (25.0 mL), respectively. With vigorous magnetic agitation, the two solutions above were quickly mixed. Then, the mixture was kept 24 h for aging under ambient conditions. Finally, centrifuged with methanol three times, the purple ZIF-67 product was obtained after drying for 10 h at 60 °C.

2.2. Synthesis of LDH Nanocages. The as-prepared ZIF-67 (90 mg) was first dispersed in ethanol (20 mL), and then the mixture of ethanol (10 mL) containing $Co(NO_3)_2{\cdot}6H_2O$ (180 mg) was quickly added to the ZIF-67 dispersion. After refluxing for 1 h under agitation, the mixture was collected through centrifugal separation with ethanol three times. The final LDH nanocages were obtained by drying in an oven for 10 h at 60 °C.

2.3. Synthesis of Co_3O_4/C Composite. A simple one-step polymerization process was used to coat the dopamine on the LDH composite. Typically, LDH nanocages (100 mg) were dispersed in a Tris-buffer aqueous solution (10 mM) under ultrasonication. Then, dopamine (50 mg) was added to the mixed solution for 12 h magnetic agitation at room temperature. LDH/PDA was obtained by centrifugal separation and then dried overnight at 60 °C. The final Co_3O_4/C composite (87 mg) was obtained by annealing the LDH/PDA composite at 500 °C for 3 h under the argon environment. For comparison, Co_3O_4 nanocages were prepared by directly annealing the LDH nanocages at 500 °C with the same treatment conditions.

2.4. Synthesis of S@Co_3O_4/C Composite. Typically, the sulfur powder was added to the Co_3O_4/C composite with an appropriate mass ratio. The mixture by milling processing was then enclosed in the Teflon autoclave for 12 h heating at 155 °C in order to infuse sulfur into the cavity of the Co_3O_4/C composite. The as-obtained product then had an additional 20 min thermal treatment at 200 °C under nitrogen, eliminating the sulfur deposited outside the composite surface. S@Co_3O_4 and S/C composites were prepared using similar processes as the S@Co_3O_4/C composite, where Co_3O_4 nanocages and carbon black acted as the sulfur hosts.

2.5. Synthesis of Li_2S_6 and Li_2S_6/Co_3O_4 Composite for Interaction Study. A lithium polysulfide solution (10 mmol L^{-1}) was synthesized as described below. Typically, lithium sulfide powder (Li_2S) and elemental sulfur (S) were mixed (molar ratio = 1:5), and then, the mixture was added to the 1,2-dimethoxyethane (DME) solvent with an equal volume of 1,3-dioxolane (DOL) under vigorous stirring for 1 day at room temperature. Then, the resulting yellow Li_2S_6 sample was obtained by washing with toluene and was then vacuum-dried. To synthesize the Li_2S_6/Co_3O_4 composite for XPS analyses, Co_3O_4 powder (20 mg) was added to the lithium polysulfide solution (5.0 mL), and the mixtures were vigorously stirred to realize sufficient adsorption. The precipitated product was centrifuged and vacuum-dried for the XPS studies.

2.6. Lithium Polysulfide Adsorption Study. Co_3O_4 nanocages and carbon black were added to the as-prepared Li_2S_6 solution separately for adsorption. A pure Li_2S_6 solution was used as a control experiment.

2.7. Materials Characterization. The materials crystallography was examined by X-ray powder diffraction (XRD, Rigaku) attached to the monochromatic Cu Kα (λ = 1.5406 Å) radiation. The sample morphology and structure were characterized using a transmission electron microscope (TEM, JEOL-JSM-2100) and scanning electron microscope (SEM, Philips/FEI XL 40 FEG). An energy-dispersive X-ray spectrometer (EDS) attached to the SEM instrument was employed to analyze the composition of the samples. Elemental mapping images were recorded using an EDS spectroscope attached to TEM. Thermogravimetric analysis (TGA, Pvris Diamond) was performed under a flow of nitrogen using a heating rate of 10 °C min^{-1}. The Raman spectrum was recorded on an HR 800 Raman spectroscopy instrument (J Y, France) with a confocal Olympus microscope and synapse CCD detector. A 633 nm He−Ne laser and 600 g mm^{-1} gratings were used by the spectrograph. X-ray photoelectron spectroscopy (XPS) measurements were performed on a Thermo Scientific K-Alpha XP spectrometer equipped with a monochromatic Al Kα X-ray source (1486.6 eV). A nitrogen adsorption−desorption isotherm investigation was conducted with a Micromeritics ASAP 2050 porosimeter to obtain the Brunauer−Emmett−Teller (BET) specific surface area. The desorption branch of the Barrett−Joyner−Halenda (BJH) model was employed to determine the pore size distribution.

DOI: 10.1021/acsaem.9b01621
ACS Appl. Energy Mater. 2019, 2, 8153−8162

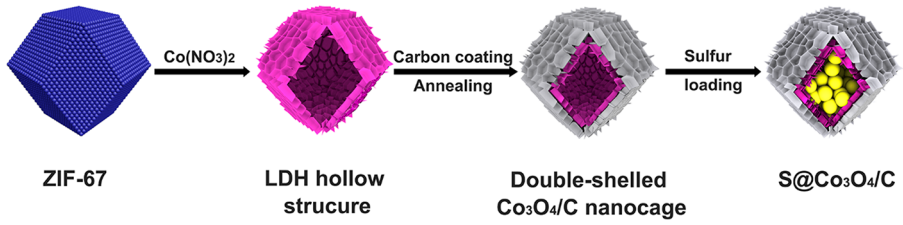

Figure 1. Schematic representation of the fabrication process of S@Co_3O_4/C composite materials.

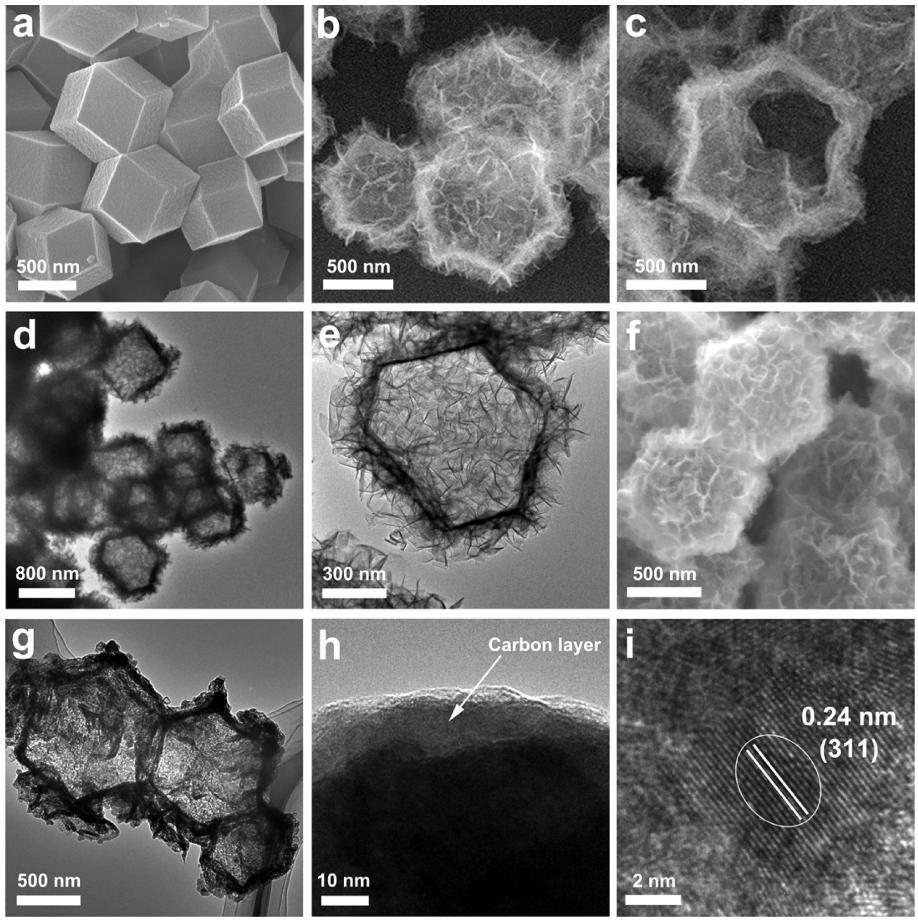

Figure 2. SEM images of (a) ZIF-67 and (b, c) LDH nanocages. (d, e) TEM images of LDH nanocages. (f) SEM image of Co_3O_4/C nanocages. (g) TEM and (h, i) HRTEM images of Co_3O_4/C nanocages.

2.8. Electrochemical Measurements. 2032-type coin cells (MTI Corp., USA) were constructed to measure the material's electrochemistry with a metallic Li foil (Sigma-Aldrich) as the counter/reference electrode, while the separator employed a polypropylene membrane (Celgard LLC., USA). The composites (80 wt %) were mixed with Super P (10 wt %) and polyvinylidene fluoride (PVDF) binder (10 wt %) in *N*-methyl pyrrolidone (NMP) solvent to form homogeneous slurries. The sulfur contents in all composites were 70 wt %, which amounted to a sulfur loading of 56 wt % in the cathodes. The resultant slurries were cast onto the carbon-coated aluminum foil (MTI Corp., USA) by a doctor-blade method and then vacuum-dried at 70 °C overnight. Finally, the working electrodes were cut into discs with the average sulfur loading of around 1.4 mg cm^{-2}. In the higher sulfur loading test, electrodes with an average sulfur loading of about 3.5 mg cm^{-2} were used. The electrolyte consisted of 1 M lithium bis(trifluoromethanesulfonyl) imide (LiTFSI) in the solvent of DOL and an equal volume of DME with 2 wt % $LiNO_3$ additive. The electrolyte volume used in each coin cell was controlled with an electrolyte/sulfur ratio of 20 μL mg^{-1}. The assembly of coin cells was performed in an argon-filled glovebox with a moisture and oxygen concentration below 5 ppm. The cells were galvanostatically measured with an M2300 galvanostat (Macoor, Tulsa, USA) from 2.7 to 1.8 V. Cyclic voltammetry (CV) was measured in the range from 1.7 to 3.0 V at 0.1 mV s^{-1}. Impedance spectroscopy (EIS) was carried out from the frequency 0.1 Hz to 200 kHz using an Autolab potentiostat. The current density was determined by the mass of pure sulfur, in which 1 C = 1675 mA g^{-1}, while the active sulfur mass was employed to calculate specific capacities.

3. RESULTS AND DISCUSSION

The synthesis strategy of the S@Co_3O_4/C composite is illustrated in Figure 1. First, highly uniform rhombic dodecahedral zeolitic imidazolate framework-67 (ZIF-67) nanoparticles were synthesized serving as the sacrificial template.[45] Then, ZIF-67 reacted with $Co(NO_3)_2$ in an ethanol solvent, transforming to hollow nanocages of layered double hydroxides (LDH). Subsequently, dopamine was employed to fabricate polydopamine (PDA) at the surface of

DOI: 10.1021/acsaem.9b01621
ACS Appl. Energy Mater. 2019, 2, 8153−8162

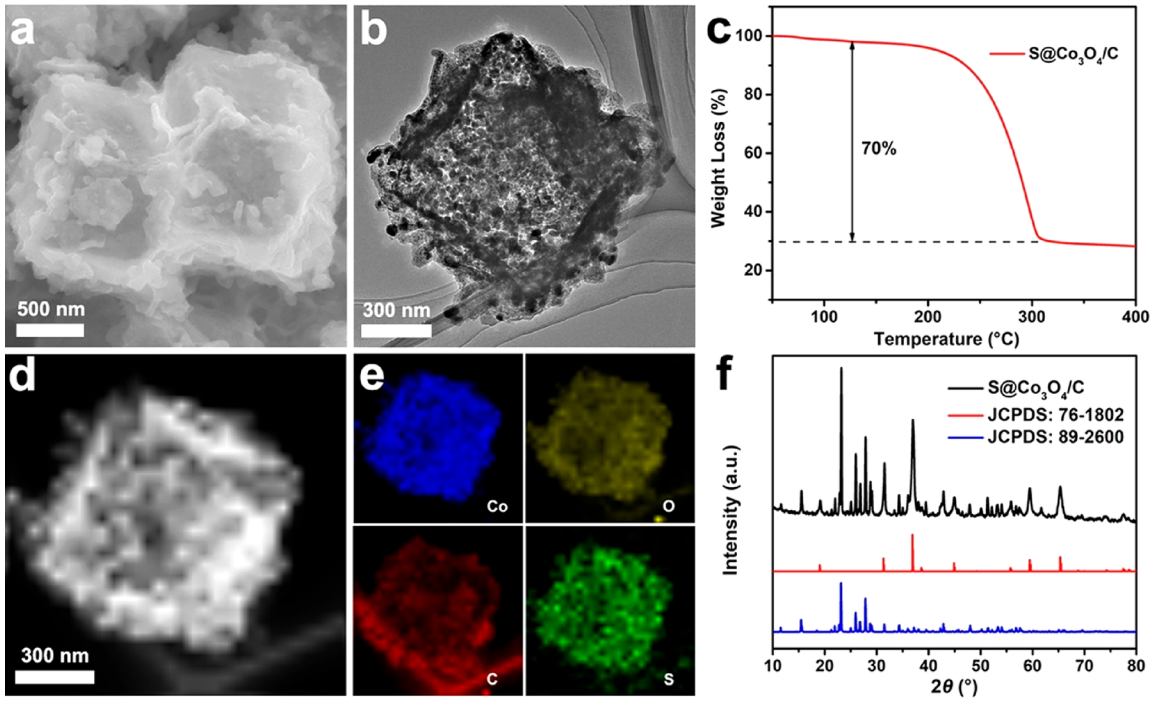

Figure 3. Characterization of the S@Co_3O_4/C composite. (a) SEM and (b) TEM images; (c) TGA curve; (d) STEM image; (e) elemental mapping of Co, O, C, and S; and (f) XRD pattern.

LDH to form double-shelled LDH/PDA nanocages.[46] The as-prepared samples were annealed, converting LDH/PDA to the Co_3O_4/C double-shelled nanocage structure. Finally, sulfur particles were encapsulated in the hollow Co_3O_4/C nanocages by melt-diffusion.

The SEM observation illustrated in Figure 2a presents the morphology of the ZIF-67 template particles. It shows the well-defined rhombic dodecahedral shape with a smooth surface, in which the size distribution remains uniform and the particle diameter is about 800 nm on average. The corresponding XRD pattern matched well the previous reports (Figure S1, Supporting Information).[47] Figure 2b shows the SEM image of LDH cages fabricated from ZIF-67. The crumpled shells assembled by tiny LDH nanosheets approximately retained the dimensions and morphology of the ZIF-67 templates. The cleft of the LDH nanocages observed in Figure 2c revealed the hollow structure. The TEM observation (Figure 2d) obviously demonstrates the hollow nanocage structure with a well-defined inner cavity. A layer of homogeneous LDH shell assembled by nanosheets can be discerned in Figure 2e. The corresponding XRD pattern (Figure S2) revealed the (003), (006), (012), and (110) peaks of a typical LDH material.[48] Subsequently, the polymerization of dopamine on the surface of the LDH nanocages generated a uniform polydopamine carbon layer. The final Co_3O_4/C nanocages with the double-shelled structure were obtained by annealing the polydopamine-coated LDH nanocages under nitrogen. Figure 2f shows the SEM image of the Co_3O_4/C nanocages with the crumpled surface. The morphology and size of the Co_3O_4/C nanocages were well-maintained. Also, the hollow structure of the cages can be clearly identified by TEM (Figure 2g). The presence of carbon shells was determined by the magnified TEM in Figure 2h with a thickness of about 10 nm, proving the existence of the double-shelled Co_3O_4/C nanocage structure. The high-resolution TEM (HRTEM) image in Figure 2i validates that the Co_3O_4 nanocages own well-defined lattice fringes with a 0.24 nm *d*-spacing, consistent with the (311) crystal plane of Co_3O_4. The XRD pattern of the Co_3O_4/C nanocages (Figure S3) shows typical diffraction peaks of Co_3O_4 (JCPDS Card 76-1802), while no significant peaks of carbon could be observed owing to the low diffraction intensity of the amorphous structure.[49,50] The Raman spectrum of the Co_3O_4/C nanocages (Figure S4a) shows two characteristic carbon peaks of the D band at around 1350 cm^{-1} and the G band at about 1550 cm^{-1}, which stem from the disordered and graphited carbon, respectively,[51,52] while the E_g, F_{2g}, and A_{1g} bands correspond to Co_3O_4. The EDS result in Figure S4b evidently signifies that Co, O, and C elements were all present in the double-shelled Co_3O_4/C nanocages. Furthermore, the homogeneous distribution of Co, O, and C elements was verified by elemental mapping of scanning transmission electron microscopy (STEM) (Figure S5).

Since the annealing temperature plays a critical role in the Co_3O_4/C structure, thermogravimetric analysis (TGA) of LDH/PDA has been performed to reveal the structural evolution. As displayed in Figure S6, the Co_3O_4/C formation occurs below 530 °C, while a significant weight loss starts near 540 °C, which might be associated with the reduction of Co_3O_4 by carbon at high temperature. The XRD patterns of the annealed products obtained at 400 and 600 °C further demonstrate the structural change (Figure S7). When annealed at 400 °C, the corresponding XRD pattern confirms the formation of the Co_3O_4/C nanocages. With the temperature increasing to 600 °C, the XRD pattern of the product shows typical diffraction peaks of cobalt (JCPDS Card 89-7093), indicating the reduction of Co_3O_4 to elemental cobalt. These results are very consistent with TGA. Therefore, annealing at 500 °C is beneficial to obtain well-defined Co_3O_4/C nanocages with highly conductive carbon shells.

DOI: 10.1021/acsaem.9b01621
ACS Appl. Energy Mater. 2019, 2, 8153−8162

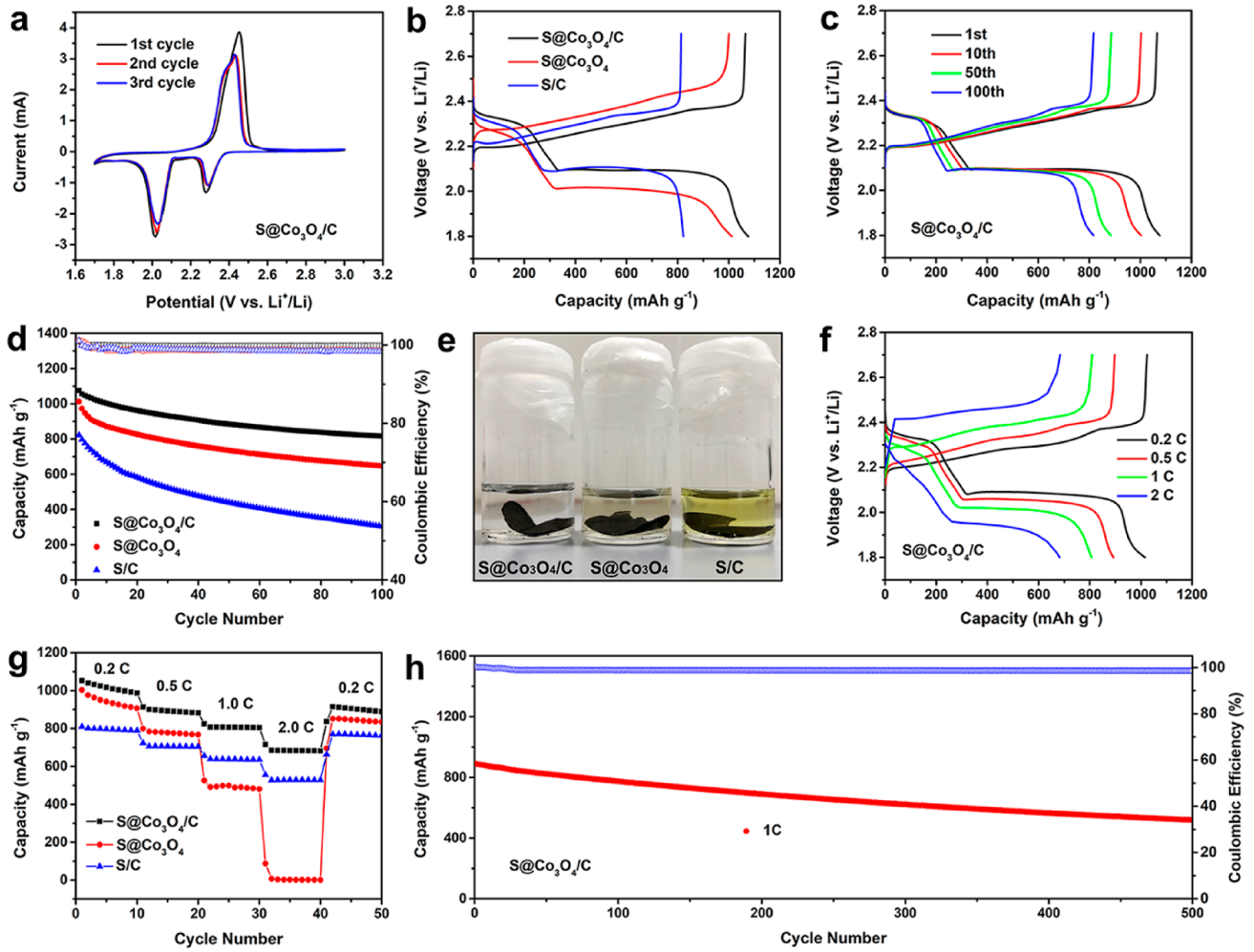

Figure 4. (a) CV curves of a S@Co_3O_4/C cathode at a scan rate of 0.1 mV s^{-1} within 1.7−3.0 V versus Li^+/Li. (b, c) Charge and discharge voltage profiles of the S@Co_3O_4/C, S@Co_3O_4, and S/C cathodes at 0.2 C. (d) Cycling performances of the three cathodes at 0.2 C. (e) Typical colors of the electrolyte for the S@Co_3O_4/C, S@Co_3O_4, and S/C cathodes after 100 cycles. (f, g) Rate capability of the three cathodes at various current densities from 0.2 to 2 C. (h) Prolonged cycle life and Coulombic efficiency of a S@Co_3O_4/C cathode at 1 C.

Sulfur was loaded into the Co_3O_4/C nanocages by a melt-diffusion method.[53] The resulting S@Co_3O_4/C composite maintained the original nanocage architecture (Figure 3a). The corresponding EDS spectrum shows a strong signal of sulfur (Figure S8), indicating a large number of sulfur particles in S@Co_3O_4/C. The TEM observation from Figure 3b demonstrates that the inner space in S@Co_3O_4/C became much darker after sulfur encapsulation, implying that sulfur particles were successfully infused into the cavities. The sulfur content in the S@Co_3O_4/C composite was determined to be 70 wt % by TGA (Figure 3c). STEM elemental mapping images indicate the homogeneous distribution of sulfur in the S@Co_3O_4/C composite (Figure 3d,e). The XRD pattern (Figure 3f) of S@Co_3O_4/C composites can be indexed to Co_3O_4 (JCPDS Card 76-1802) and sulfur (JCPDS Card 89-2600), implying good consistency of peaks after sulfur loading into Co_3O_4/C nanocages. The nitrogen adsorption−desorption measurements demonstrate the change in pore volumes of Co_3O_4/C after sulfur loading. As shown in Figure S9, the BET surface area of Co_3O_4/C nanocages was measured to be as high as 306.11 m^2 g^{-1}, and the calculated pore volume reached 0.594 cm^3 g^{-1}. With sulfur loading, the surface area of S@Co_3O_4/C dropped to 10.56 m^2 g^{-1} while a distinct decline in the pore volume occurred (only 0.072 cm^3 g^{-1} after sulfur loading), implying that sulfur had infused the majority of pores. All these results confirm that sulfur has been infused into the cavities of Co_3O_4/C nanocages.

The S@Co_3O_4/C composite was fabricated to be a sulfur cathode for evaluating the electrochemical performance. In order to determine the structural merits of the S@Co_3O_4/C composite materials, S@Co_3O_4, and S/C composites were prepared using Co_3O_4 nanocages and carbon black as the hosts, respectively. Their electrochemical performances were also evaluated for comparison. In all three samples, the sulfur mass loading was 70 wt % confirmed by TGA (Figure 3c and Figure S10). The CV curves of S@Co_3O_4/C illustrated in Figure 4a reveal the typical redox process of Li−S batteries. Two reduction peaks emerge during lithiation and arise from the transformation from elemental sulfur to soluble polysulfides (Li_2S_n, $4 \leq n \leq 8$) and ultimately to solid Li_2S_2 and Li_2S sulfides, while the oxidation peak during delithiation can be associated with the reverse reaction.[54] In the following two cycles, the two reduction peaks slightly shifted toward more positive potentials and the oxidation peak toward more negative potentials, implying the mitigation of polarization and the improvement of electrochemical charge transfer kinetics. These variations mainly arise from the rearrangement of the active sulfur upon cycling, resulting in more energetically

DOI: 10.1021/acsaem.9b01621
ACS Appl. Energy Mater. 2019, 2, 8153−8162

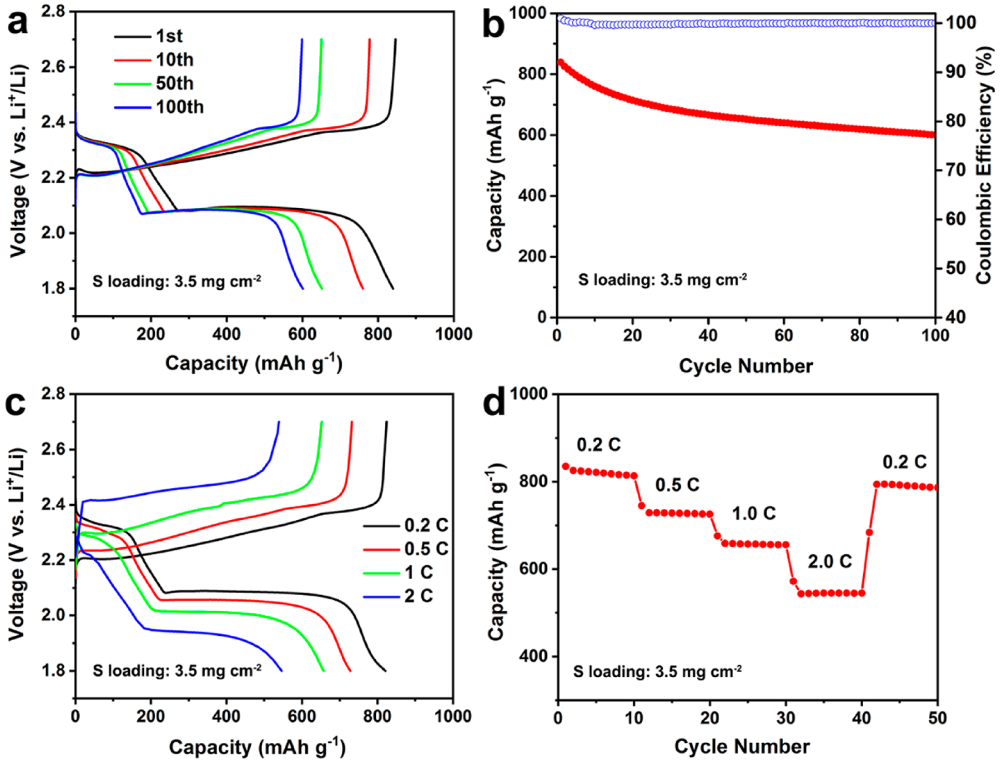

Figure 5. (a) Charge and discharge voltage profiles and (b) cycling performance of S@Co_3O_4/C with a sulfur loading of 3.5 mg cm^{-2} at 0.2 C. (c, d) Rate capability of S@Co_3O_4/C with a sulfur loading of 3.5 mg cm^{-2} at various current densities from 0.2 to 2 C.

stable sulfur particles.[55] The good consistency of the oxidation and reduction peaks in the two consecutive cycles indicates the good electrochemical stability of S@Co_3O_4/C.

EIS analyses were conducted in order to additionally demonstrate the structural superiority of the S@Co_3O_4/C cathode. The EIS equivalent circuit is presented in Figure S11 with the parameter results in Table S1. As displayed in Figure S11, the Nyquist plots reveal that each of the three composite electrodes comprised a depressed semicircle and a declined line located in the regions of high and low frequencies, representing the charge transfer process on the interface of the cathode/electrolyte and semi-infinite Warburg diffusion in the sulfur cathode, respectively.[56,57] The intercept with the real axis is associated with the cell resistance.[58] The S@Co_3O_4/C cathode exhibited the smallest semicircle, indicating the lowest charge transfer resistance (R_{ct}) and enhanced redox kinetics. From the CV and EIS results, it can be concluded that the double-shelled Co_3O_4/C nanocage structure can significantly boost the cycling life and ensure the high rate capability, because of the efficient adsorption of active sulfur species as well as considerable acceleration of the charge transfer kinetics.

Figure 4b presents the charge and discharge voltage profiles of three composites cathodes at 0.2 C. All three cells exhibited well-defined discharge plateaus at the potential around 2.3 and 2.1 V, consistent with a typical discharging curve of a Li−S battery.[59] The electrochemical polarization upon cycling can be determined from the plateau voltage gap (ΔV). Among the three electrodes, S@Co_3O_4/C exhibited the narrowest voltage gap (i.e., the smallest polarization) and highest low-voltage plateau capacity, indicating fast charge transfer kinetics and effective utilization of active sulfur species in the S@Co_3O_4/C cathode. The cycling performance of S@Co_3O_4/C, S@Co_3O_4, and S/C was compared at 0.2 C in Figure 4c,d, and Figure S12. Due to the structural superiority, the S@Co_3O_4/C cathode initially attained a capacity of 1076 mAh g^{-1}. On the other hand, the S@Co_3O_4 and S/C cathodes only reached 1012 and 822 mAh g^{-1}, respectively. Furthermore, S@Co_3O_4/C still delivered a capacity of about 817 mAh g^{-1} after 100 cycles at 0.2 C, which was equivalent to the capacity retention of 75.9%, whereas S@Co_3O_4 and S/C cathodes only delivered 647 and 304 mAh g^{-1}, respectively, indicating that only initial capacities of 63.9% and 37.2% were maintained. In addition, the S@Co_3O_4/C cathode exhibited the highest Coulombic efficiency among the three electrodes. Pure Co_3O_4/C nanocage cathodes without sulfur were conducted to determine their capacity contribution. As shown in Figure S13, in a same test situation, pure Co_3O_4/C nanocages only delivered not more than 10 mAh g^{-1} during 100 cycles.

Furthermore, the three composite electrodes after 100 cycles were separately soaked in a solvent consisting of 1,2-dimethoxyethane (DME) and an equal volume of 1,3-dioxolane (DOL) to observe the diffusion of polysulfides. As shown in Figure 4e, the solvents containing S@Co_3O_4/C and S@Co_3O_4 cathodes nearly kept their initial colors, whereas the color of the solution with S/C cathode turned into yellow. This color observation clearly indicates that Co_3O_4 nanocage structures can efficiently prevent polysulfides from diffusing into the electrolyte. The highest initial discharge capacity and favorable cycling stability of S@Co_3O_4/C benefit from the synergetic functions of the double-shelled nanocages by better anchoring the lithium polysulfides and facilitating enhanced redox kinetics, contributing to sufficient utilization of active sulfur species. To further reveal the advantages of the Co_3O_4/C nanocages for the polysulfide adsorption, cycled lithium metal anodes were disassembled from the three composite cells for comparison (Figure S14). The lithium foils from the S@

DOI: 10.1021/acsaem.9b01621
ACS Appl. Energy Mater. 2019, 2, 8153−8162

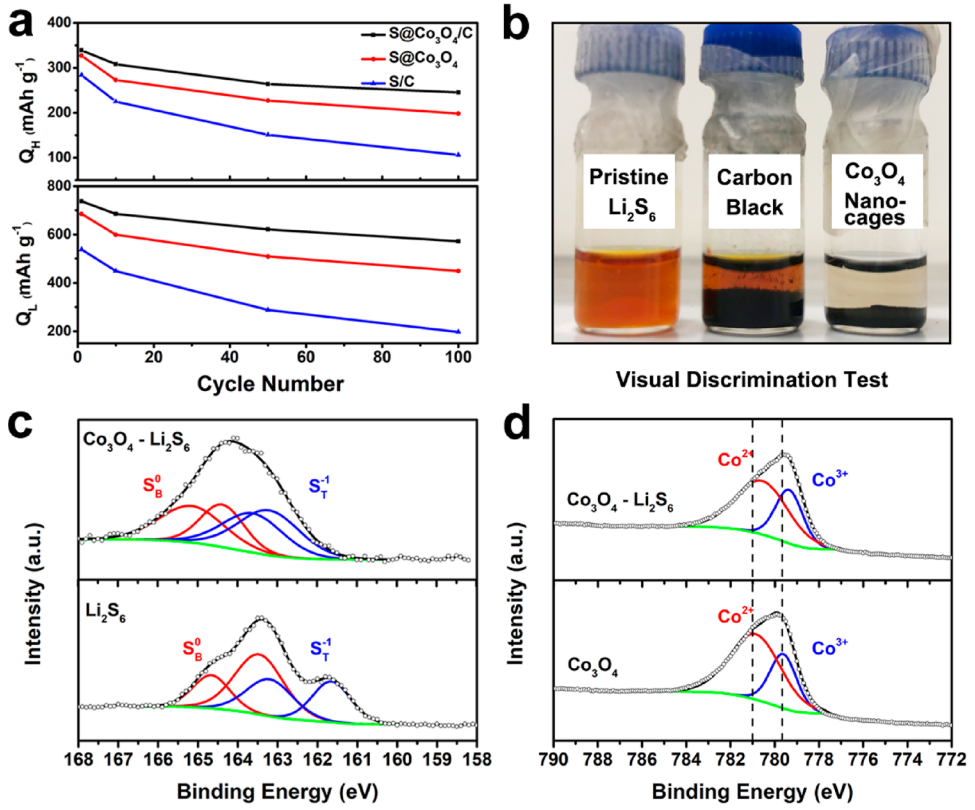

Figure 6. (a) Capacities of Q_H and Q_L of S@Co_3O_4/C, S@Co_3O_4, and S/C cathodes at 0.2 C at various indicated cycles. (b) Static adsorption of Li_2S_6 with carbon black and Co_3O_4 nanocages after 6 h. High-resolution XPS spectra of the interaction between Li_2S_6 and Co_3O_4: (c) S 2p of Li_2S_6 and Co_3O_4–Li_2S_6; (d) Co 2p of Co_3O_4 and Co_3O_4–Li_2S_6.

Co_3O_4/C and S@Co_3O_4 cells show a smooth surface, and the morphology was preserved, indicating that the dissolution of polysulfides has been significantly inhibited. However, the lithium foil of the S/C cell presents an obviously rough surface. The severe erosion of the lithium foil was clearly ascribed to the shuttle issue of polysulfides. In addition, the cycled S@Co_3O_4/C composite cathode maintained well the morphology and structure, indicating good stability of the S@Co_3O_4/C composite upon cycling (Figure S15).

The rate capabilities of the three composite electrodes were investigated in the range from 0.2 to 2 C (Figure 4f,g, and Figure S16). With regard to the S@Co_3O_4/C cathode, two typical discharge plateaus can be discerned even up to 2 C, implying significant polarization mitigation. This cathode attained a highly stable discharge capacity of 1017 mAh g^{-1} at 0.2 C. With a progressive increase in current density, the discharge capacities of S@Co_3O_4/C remained steady at 893 (0.5 C), 807 (1 C), and 682 (2 C) mAh g^{-1}, respectively. Moreover, S@Co_3O_4/C reached a highly stable capacity of 905 mAh g^{-1} after the current density dropped to 0.2 C, meaning that S@Co_3O_4/C had favorable rate capability and electrode stability. On the other hand, the S/C cathode exhibited distinctly inferior discharge capacities at various current densities, mainly resulting from the loss of polysulfides upon cycling; the S@Co_3O_4 cathode suffered a dramatic drop in capacity at 1 C, implying a relatively poor charge transfer due to the absence of carbon. The rate capabilities of the three cathodes are very consistent with the EIS results discussed above.

The prolonged cycling stability of the S@Co_3O_4/C composite cathode was further investigated at 1 C, which is illustrated in Figure 4h. The S@Co_3O_4/C cathode initially delivered a reversible capacity of 889 mAh g^{-1} and maintained 520 mAh g^{-1} after a 500-cycle discharging and changing process. Low capacity fading of 0.083% per cycle was achieved accompanied by a corresponding Coulombic efficiency of about 99% during the whole cycling process. This superior long-term stability achieved by the S@Co_3O_4/C composite cathodes can rival most metal oxides, carbonaceous composites, and hybrid electrodes reported before (Tables S2).

Since high sulfur loading enables Li–S batteries with high energy density for commercialization applications, an S@Co_3O_4/C cathode containing higher sulfur loading up to 3.5 mg cm^{-2} was further assessed. Figure 5a,b presents the resulting voltage profiles and cycling curves at 0.2 C. The high-load S@Co_3O_4/C cathodes initially delivered a high capacity of 839 mAh g^{-1}. Even with a 100-cycle discharging process, a steady capacity of 601 mAh g^{-1} was still attained. The increase in sulfur loading barely incurs the aggravation of polarization, implying good electrochemical kinetics and cycling life. Furthermore, the S@Co_3O_4/C cathodes also exhibit impressive rate capabilities at high current rates (Figure 5c,d). Reversible capacities of 821 (0.2 C), 728 (0.5 C), 657 (1 C), and 546 mAh g^{-1} (2 C) were achieved. S@Co_3O_4/C still attained a stable capacity of 792 mAh g^{-1} when the current density fell to 0.2 C. These results firmly demonstrate that the S@Co_3O_4/C cathodes offer the potential for practical Li–S batteries.

In order to evaluate the adsorption capability of Co_3O_4 nanocages for lithium polysulfide species, the upper-plateau (Q_H) and lower-plateau (Q_L) capacities extracted from the discharge voltage profiles were investigated. Q_H corresponds to

DOI: 10.1021/acsaem.9b01621
ACS Appl. Energy Mater. 2019, 2, 8153–8162

the fast solid-to-liquid transformation from sulfur to soluble polysulfides, which mainly determine the capacity retention and cathode stability due to the polysulfide diffusion and migration.[60,61] Q_L involves the slow liquid-to-solid conversion from soluble polysulfides to insoluble species. The Q_H and Q_L theoretical capacities are 419 and 1256 mAh g^{-1}, respectively.[62] The specific Q_H and Q_L values of S@Co_3O_4/C, S@Co_3O_4, and S/C cycling at 0.2 C were listed in Table S3. As illustrated in Figure 6a, S@Co_3O_4/C can deliver an initial Q_H value of 339 mAh g^{-1} and then exhibit a relatively high Q_H value after 100 cycles, achieving the high average Q_H retention rate (R_{QH}) of 72%. Similarly, the S@Co_3O_4 cathode also exhibits a high R_{QH} value of 61% after 100 cycles. By contrast, S/C reveals an obviously low initial Q_H value of 284 mAh g^{-1} and R_{QH} value of 37% under the same conditions. Accordingly, the S@Co_3O_4/C and S@Co_3O_4 cathodes show considerably higher Q_L capacities and Q_L retention rate (R_{QL}) than the S/C cathode, implying that the adsorbed polysulfides by Co_3O_4 nanocages can adequately be converted to the end-discharge products upon cycling. These results clearly demonstrate that the prepared Co_3O_4 nanocages possess superior polysulfide adsorption capability, which can noticeably inhibit the shuttle problem of polysulfides.

A visual discrimination test was conducted to confirm the strong adsorption of prepared Co_3O_4 nanocages for lithium polysulfides. Li_2S_6 was conducted as the representative of polysulfide species, which was synthesized according to the previous report.[63] Co_3O_4 nanocages and carbon black were separately dispersed into a Li_2S_6 solution of 10.0 mmol L^{-1}, followed by vigorous stirring to induce good adsorption. As demonstrated in Figure 6b, the solution with Co_3O_4 nanocages is nearly transparent because of the complete adsorption of Li_2S_6. On the contrary, the solution with carbon black is virtually unchanged in color. This observation again indicates the considerable adsorption of prepared Co_3O_4 nanocages toward lithium polysulfides. In addition, XPS analyses further demonstrate the chemical interaction between Co_3O_4 and Li_2S_6. Figure 6c shows the S 2p spectra of pristine Li_2S_6 and Li_2S_6/Co_3O_4. The pristine Li_2S_6 spectrum exhibited two contributions of S 2p at 161.6 and 163.4 eV, assigned to terminal sulfur (S_T^{-1}) and bridging sulfur atoms (S_B^0), respectively.[64] The S_T^{-1} contribution of Li_2S_6/Co_3O_4, by contrast, shifted more than 0.5 eV to higher binding energies, indicative of electron transfer from Li_2S_6 to Co_3O_4 due to chemical interaction. Accordingly, in the Co $2p_{3/2}$ spectra (Figure 6d), the Co $2p_{1/2}$ and Co $2p_{3/2}$ spectra of Li_2S_6/Co_3O_4 shifted toward lower binding energies compared with those of pristine Co_3O_4.[65] Overall, the XPS analyses clearly demonstrate the strong chemical interaction between the Li_2S_6 and Co_3O_4.

The outstanding electrochemical performance of S@Co_3O_4/C derives from the following advantages. First, the Co_3O_4 nanocage structure can effectively anchor the lithium polysulfides by the strong chemical interaction of Li−O and S−Co bonds, which is supported by Q_H and Q_L analyses, static adsorption of polysulfides, and XPS investigations. The beneficial interaction between polar Co_3O_4 and polysulfide intermediates facilitates mitigation of the loss of active sulfur species, resulting in better cycling life. In addition, the excellent conductivity of the carbon shells significantly improves the composite cathode with better charge transfer capability. Specifically, the electrochemical polarization of S@Co_3O_4/C observed in the CV curves and voltage profiles (Figure 4a,b) is evidently smaller than that of the other two electrodes. This indicates a more favorable charge transfer kinetics for the S@Co_3O_4/C cathode, causing a better rate capability (Figure 4f,g). Finally, the double-shelled nanocage structure provides a three-dimensional pathway, which can be readily accessed by electrons and lithium ions. As a result, the robust structure of the S@Co_3O_4/C composite, in combination with the effective adsorption to lithium polysulfides and high conductivity, contributes to excellent electrochemical performance for sulfur cathodes.

4. CONCLUSIONS

In summary, we have demonstrated a novel design to fabricate double-shelled Co_3O_4 and carbon hollow nanocage sulfur host materials. Due to the synergetic effect of the double-shelled Co_3O_4/C nanocage structure, the Co_3O_4/C sulfur host can effectively adsorb polysulfides and facilitate charge transfer, thus inhibiting the diffusion and migration of polysulfides and improving the electrochemical kinetics of the cathode. Q_H and Q_L analyses, static adsorption of polysulfides, and XPS investigations validate the chemical interactions between polysulfides and Co_3O_4 nanocages. Benefiting from the structural superiority, the S@Co_3O_4/C composite electrode achieved a favorable capacity at 0.2 C, superior cycling stability with capacity fading just 0.083% per cycle at 1 C, and impressive rate performance. The present results broaden the understanding of chemical interactions between lithium polysulfides and polar materials and favor the design and screening of prospective structures for enhanced performance of Li−S batteries.

■ ASSOCIATED CONTENT

Supporting Information

The Supporting Information is available free of charge on the ACS Publications website at DOI: 10.1021/acsaem.9b01621.

Additional figures including SEM, TEM, Raman, TG curves, XRD data, and additional electrochemical and characterization data (PDF)

■ AUTHOR INFORMATION

Corresponding Author

*E-mail: p.h.l.notten@tue.nl (P.H.L.N.).

ORCID

Lei Zhou: 0000-0003-0222-9469

Peter H. L. Notten: 0000-0003-4907-8426

Notes

The authors declare no competing financial interest.

■ ACKNOWLEDGMENTS

The authors L.Z., X.W., and Y.Z. acknowledge the financial support of the China Scholarship Council.

■ REFERENCES

(1) Armand, M.; Tarascon, J. M. Building better batteries. *Nature* **2008**, *451*, 652−657.

(2) Tarascon, J. M.; Armand, M. Issues and challenges facing rechargeable lithium batteries. *Nature* **2001**, *414*, 359−367.

(3) Bruce, P. G.; Freunberger, S. A.; Hardwick, L. J.; Tarascon, J. M. Li-O_2 and Li-S batteries with high energy storage. *Nat. Mater.* **2012**, *11*, 19−29.

(4) Manthiram, A.; Fu, Y.; Su, Y. Challenges and prospects of lithium-sulfur batteries. *Acc. Chem. Res.* **2013**, *46*, 1125−1134.

DOI: 10.1021/acsaem.9b01621
ACS Appl. Energy Mater. 2019, 2, 8153−8162

(5) He, J.; Manthiram, A. A review on the status and challenges of electrocatalysts in lithium-sulfur batteries. *Energy Storage Mater.* **2019**, *20*, 55−70.
(6) Ji, X.; Lee, K. T.; Nazar, L. F. A highly ordered nanostructured carbon−sulphur cathode for lithium−sulphur batteries. *Nat. Mater.* **2009**, *8*, 500−506.
(7) Zhang, Q.; Wang, Y.; Seh, Z. W.; Fu, Z.; Zhang, R.; Cui, Y. Understanding the anchoring effect of two-dimensional layered materials for lithium-sulfur batteries. *Nano Lett.* **2015**, *15*, 3780−6.
(8) Li, Z.; Huang, Y.; Yuan, L.; Hao, Z.; Huang, Y. Status and prospects in sulfur−carbon composites as cathode materials for rechargeable lithium−sulfur batteries. *Carbon* **2015**, *92*, 41−63.
(9) Zu, C.; Manthiram, A. Hydroxylated graphene-sulfur nanocomposites for high-rate lithium-sulfur batteries. *Adv. Energy Mater.* **2013**, *3*, 1008−1012.
(10) Tang, H.; Yang, J.; Zhang, G.; Liu, C.; Wang, H.; Zhao, Q.; Hu, J.; Duan, Y.; Pan, F. Self-assembled N-graphene nanohollows enabling ultrahigh energy density cathode for Li-S batteries. *Nanoscale* **2018**, *10*, 386−395.
(11) Kong, L.; Li, B.-Q.; Peng, H.-J.; Zhang, R.; Xie, J.; Huang, J.-Q.; Zhang, Q. Porphyrin-derived graphene-based nanosheets enabling strong polysulfide chemisorption and rapid kinetics in lithium-sulfur batteries. *Adv. Energy Mater.* **2018**, *8*, 1800849.
(12) Peng, H.-J.; Liang, J.; Zhu, L.; Huang, J.-Q.; Cheng, X.-B.; Guo, X.; Ding, W.; Zhu, W.; Zhang, Q. Catalytic self-limited assembly at hard templates: a mesoscale approach to graphene nanoshells for lithium−sulfur batteries. *ACS Nano* **2014**, *8*, 11280−11289.
(13) Guo, J.; Xu, Y.; Wang, C. Sulfur-impregnated disordered carbon nanotubes cathode for lithium-sulfur batteries. *Nano Lett.* **2011**, *11*, 4288−94.
(14) Xu, G.; Kushima, A.; Yuan, J.; Dou, H.; Xue, W.; Zhang, X.; Yan, X.; Li, J. Ad hoc solid electrolyte on acidized carbon nanotube paper improves cycle life of lithium−sulfur batteries. *Energy Environ. Sci.* **2017**, *10*, 2544−2551.
(15) Cheng, X.-B.; Huang, J.-Q.; Zhang, Q.; Peng, H.-J.; Zhao, M.-Q.; Wei, F. Aligned carbon nanotube/sulfur composite cathodes with high sulfur content for lithium−sulfur batteries. *Nano Energy* **2014**, *4*, 65−72.
(16) He, J.; Chen, Y.; Lv, W.; Wen, K.; Xu, C.; Zhang, W.; Qin, W.; He, W. Three-dimensional CNT/graphene-Li_2S aerogel as free-standing cathode for high-performance Li−S batteries. *ACS Energy Lett.* **2016**, *1*, 820−826.
(17) Pei, F.; Lin, L.; Ou, D.; Zheng, Z.; Mo, S.; Fang, X.; Zheng, N. Self-supporting sulfur cathodes enabled by two-dimensional carbon yolk-shell nanosheets for high-energy-density lithium-sulfur batteries. *Nat. Commun.* **2017**, *8*, 482.
(18) Li, W.; Zheng, G.; Yang, Y.; Seh, Z. W.; Liu, N.; Cui, Y. High-performance hollow sulfur nanostructured battery cathode through a scalable, room temperature, one-step, bottom-up approach. *Proc. Natl. Acad. Sci. U. S. A.* **2013**, *110*, 7148−7153.
(19) Li, G.; Sun, J.; Hou, W.; Jiang, S.; Huang, Y.; Geng, J. Three-dimensional porous carbon composites containing high sulfur nanoparticle content for high-performance lithium-sulfur batteries. *Nat. Commun.* **2016**, *7*, 10601.
(20) Chen, C.; Li, D.; Gao, L.; Harks, P. P. R. M. L.; Eichel, R.-A.; Notten, P. H. L. Carbon-coated core−shell Li_2S@C nanocomposites as high performance cathode materials for lithium−sulfur batteries. *J. Mater. Chem. A* **2017**, *5*, 1428−1433.
(21) Zhang, H.; Zhao, Z.; Liu, Y.; Liang, J.; Hou, Y.; Zhang, Z.; Wang, X.; Qiu, J. Nitrogen-doped hierarchical porous carbon derived from metal−organic aerogel for high performance lithium−sulfur batteries. *J. Energy Chem.* **2017**, *26*, 1282−1290.
(22) He, J.; Luo, L.; Chen, Y.; Manthiram, A. Yolk−shelled C@Fe_3O_4 nanoboxes as efficient sulfur hosts for high-performance lithium-sulfur batteries. *Adv. Mater.* **2017**, *29*, 1702707.
(23) Li, Z.; Zhang, J.; Guan, B.; Wang, D.; Liu, L. M.; Lou, X. W. A sulfur host based on titanium monoxide@carbon hollow spheres for advanced lithium-sulfur batteries. *Nat. Commun.* **2016**, *7*, 13065.
(24) Kong, L.; Chen, X.; Li, B. Q.; Peng, H. J.; Huang, J. Q.; Xie, J.; Zhang, Q. A bifunctional perovskite promoter for polysulfide regulation toward stable lithium-sulfur batteries. *Adv. Mater.* **2018**, *30*, 1705219.
(25) Tang, W.; Zhang, Y.; Zhong, W.; Aslam, M. K.; Guo, B.; Bao, S. J.; Xu, M. A labyrinth-like network electrode design for lithium-sulfur batteries. *Nanoscale* **2019**, *11*, 14648−14653.
(26) Jiang, J.; Zhu, J.; Ai, W.; Wang, X.; Wang, Y.; Zou, C.; Huang, W.; Yu, T. Encapsulation of sulfur with thin-layered nickel-based hydroxides for long-cyclic lithium-sulfur cells. *Nat. Commun.* **2015**, *6*, 8622.
(27) Peng, H. J.; Zhang, Z. W.; Huang, J. Q.; Zhang, G.; Xie, J.; Xu, W. T.; Shi, J. L.; Chen, X.; Cheng, X. B.; Zhang, Q. A cooperative interface for highly efficient lithium-sulfur batteries. *Adv. Mater.* **2016**, *28*, 9551−9558.
(28) Zhang, J.; Li, Z.; Chen, Y.; Gao, S.; Lou, X. W. D. Nickel-iron layered double hydroxide hollow polyhedrons as a superior sulfur host for lithium-sulfur batteries. *Angew. Chem., Int. Ed.* **2018**, *57*, 10944−10948.
(29) Dai, C.; Hu, L.; Wang, M.-Q.; Chen, Y.; Han, J.; Jiang, J.; Zhang, Y.; Shen, B.; Niu, Y.; Bao, S.-J.; Xu, M. Uniform α-$Ni(OH)_2$ hollow spheres constructed from ultrathin nanosheets as efficient polysulfide mediator for long-term lithium-sulfur batteries. *Energy Storage Mater.* **2017**, *8*, 202−208.
(30) Zhang, J.; Hu, H.; Li, Z.; Lou, X. W. Double-shelled nanocages with cobalt hydroxide inner shell and layered double hydroxides outer shell as high-efficiency polysulfide mediator for lithium-sulfur batteries. *Angew. Chem., Int. Ed.* **2016**, *55*, 3982−6.
(31) Chen, T.; Ma, L.; Cheng, B.; Chen, R.; Hu, Y.; Zhu, G.; Wang, Y.; Liang, J.; Tie, Z.; Liu, J.; Jin, Z. Metallic and polar Co_9S_8 inlaid carbon hollow nanopolyhedra as efficient polysulfide mediator for lithium−sulfur batteries. *Nano Energy* **2017**, *38*, 239−248.
(32) Dai, C.; Lim, J.-M.; Wang, M.; Hu, L.; Chen, Y.; Chen, Z.; Chen, H.; Bao, S.-J.; Shen, B.; Li, Y.; Henkelman, G.; Xu, M. Honeycomb-like spherical cathode host constructed from hollow metallic and polar Co_9S_8 tubules for advanced lithium-sulfur batteries. *Adv. Funct. Mater.* **2018**, *28*, 1704443.
(33) Hu, L.; Dai, C.; Lim, J. M.; Chen, Y.; Lian, X.; Wang, M.; Li, Y.; Xiao, P.; Henkelman, G.; Xu, M. A highly efficient double-hierarchical sulfur host for advanced lithium-sulfur batteries. *Chem. Sci.* **2018**, *9*, 666−675.
(34) Guo, B.; Bandaru, S.; Dai, C.; Chen, H.; Zhang, Y.; Xu, Q.; Bao, S.; Chen, M.; Xu, M. Self-supported $FeCo_2S_4$ nanotube arrays as binder-free cathodes for lithium-sulfur batteries. *ACS Appl. Mater. Interfaces* **2018**, *10*, 43707−43715.
(35) Dai, C.; Hu, L.; Li, X.; Xu, Q.; Wang, R.; Liu, H.; Chen, H.; Bao, S.-J.; Chen, Y.; Henkelman, G.; Li, C. M.; Xu, M. Chinese knot-like electrode design for advanced Li-S batteries. *Nano Energy* **2018**, *53*, 354−361.
(36) He, J.; Chen, Y.; Manthiram, A. Metal Sulfide-decorated carbon sponge as a highly efficient electrocatalyst and absorbant for polysulfide in high-loading Li_2S batteries. *Adv. Energy Mater.* **2019**, *9*, 1900584.
(37) He, J.; Hartmann, G.; Lee, M.; Hwang, G. S.; Chen, Y.; Manthiram, A. Freestanding 1T MoS_2/graphene heterostructures as a highly efficient electrocatalyst for lithium polysulfides in Li-S batteries. *Energy Environ. Sci.* **2019**, *12*, 344−350.
(38) Pang, Q.; Kundu, D.; Nazar, L. F. A graphene-like metallic cathode host for long-life and high-loading lithium−sulfur batteries. *Mater. Horiz.* **2016**, *3*, 130−136.
(39) Xiao, Z.; Yang, Z.; Zhou, L.; Zhang, L.; Wang, R. Highly conductive porous transition metal dichalcogenides via water steam etching for high-performance lithium-sulfur batteries. *ACS Appl. Mater. Interfaces* **2017**, *9*, 18845−18855.
(40) Li, Y.-J.; Fan, J.-M.; Zheng, M.-S.; Dong, Q.-F. A novel synergistic composite with multi-functional effects for high-performance Li−S batteries. *Energy Environ. Sci.* **2016**, *9*, 1998−2004.
(41) Zhao, R.; Liang, Z.; Zou, R.; Xu, Q. Metal-organic frameworks for batteries. *Joule* **2018**, *2*, 2235.

DOI: 10.1021/acsaem.9b01621
ACS Appl. Energy Mater. 2019, 2, 8153−8162

(42) He, J.; Chen, Y.; Lv, W.; Wen, K.; Xu, C.; Zhang, W.; Li, Y.; Qin, W.; He, W. From metal-organic framework to Li_2S@C-Co-N nanoporous architecture: a high-capacity cathode for lithium-sulfur batteries. *ACS Nano* **2016**, *10*, 10981−10987.
(43) Chang, Z.; Dou, H.; Ding, B.; Wang, J.; Wang, Y.; Hao, X.; MacFarlane, D. R. Co_3O_4 nanoneedle arrays as a multifunctional "super-reservoir" electrode for long cycle life Li−S batteries. *J. Mater. Chem. A* **2017**, *5*, 250−257.
(44) Xu, J.; Zhang, W.; Chen, Y.; Fan, H.; Su, D.; Wang, G. MOF-derived porous N−Co_3O_4@N−C nanododecahedra wrapped with reduced graphene oxide as a high capacity cathode for lithium−sulfur batteries. *J. Mater. Chem. A* **2018**, *6*, 2797−2807.
(45) Jiang, Z.; Li, Z.; Qin, Z.; Sun, H.; Jiao, X.; Chen, D. LDH nanocages synthesized with MOF templates and their high performance as supercapacitors. *Nanoscale* **2013**, *5*, 11770−5.
(46) Lee, H.; Dellatore, S. M.; Miller, W. M.; Messersmith, P. B. Mussel-inspired surface chemistry for multifunctional coatings. *Science* **2007**, *318*, 426−430.
(47) Xia, W.; Zhu, J.; Guo, W.; An, L.; Xia, D.; Zou, R. Well-defined carbon polyhedrons prepared from nano metal−organic frameworks for oxygen reduction. *J. Mater. Chem. A* **2014**, *2*, 11606.
(48) Hu, Z.-A.; Xie, Y.-L.; Wang, Y.-X.; Wu, H.-Y.; Yang, Y.-Y.; Zhang, Z.-Y. Synthesis and electrochemical characterization of mesoporous Co_xNi_{1-x} layered double hydroxides as electrode materials for supercapacitors. *Electrochim. Acta* **2009**, *54*, 2737−2741.
(49) Liang, Y.; Li, Y.; Wang, H.; Zhou, J.; Wang, J.; Regier, T.; Dai, H. Co_3O_4 nanocrystals on graphene as a synergistic catalyst for oxygen reduction reaction. *Nat. Mater.* **2011**, *10*, 780−786.
(50) Chen, J.; Xia, X.-H.; Tu, J.-P.; Xiong, Q.-Q.; Yu, Y.-X.; Wang, X.-L.; Gu, C.-D. Co_3O_4−C core−shell nanowire array as an advanced anode material for lithium ion batteries. *J. Mater. Chem.* **2012**, *22*, 15056.
(51) Tuinstra, F.; Koenig, J. L. Raman spectrum of graphite. *J. Chem. Phys.* **1970**, *53*, 1126.
(52) Zhou, L.; Liu, J.; Zhang, X.; Liu, R.; Huang, H.; Liu, Y.; Kang, Z. Template-free fabrication of mesoporous carbons from carbon quantum dots and their catalytic application to the selective oxidation of hydrocarbons. *Nanoscale* **2014**, *6*, 5831−5837.
(53) Cui, Z.; Zu, C.; Zhou, W.; Manthiram, A.; Goodenough, J. B. Mesoporous titanium nitride-enabled highly stable lithium-sulfur batteries. *Adv. Mater.* **2016**, *28*, 6926−31.
(54) Yang, Y.; Zheng, G.; Cui, Y. Nanostructured sulfur cathodes. *Chem. Soc. Rev.* **2013**, *42*, 3018−3032.
(55) Shan, J.; Liu, Y.; Su, Y.; Liu, P.; Zhuang, X.; Wu, D.; Zhang, F.; Feng, X. Graphene-directed two-dimensional porous carbon frameworks for high-performance lithium−sulfur battery cathodes. *J. Mater. Chem. A* **2016**, *4*, 314−320.
(56) Park, S.-K.; Lee, J.-K.; Kang, Y. C. Yolk-shell structured assembly of bamboo-like nitrogen-doped carbon nanotubes embedded with Co nanocrystals and their application as cathode material for Li-S batteries. *Adv. Funct. Mater.* **2018**, *28*, 1705264.
(57) Li, W.; Zhang, Q.; Zheng, G.; Seh, Z. W.; Yao, H.; Cui, Y. Understanding the role of different conductive polymers in improving the nanostructured sulfur cathode performance. *Nano Lett.* **2013**, *13*, 5534−40.
(58) Kazazi, M.; Vaezi, M. R.; Kazemzadeh, A. Enhanced rate performance of polypyrrole-coated sulfur/MWCNT cathode material: a kinetic study by electrochemical impedance spectroscopy. *Ionics* **2014**, *20*, 635−643.
(59) Zhang, S. S. Liquid electrolyte lithium/sulfur battery: Fundamental chemistry, problems, and solutions. *J. Power Sources* **2013**, *231*, 153−162.
(60) Chang, C.-H.; Chung, S.-H.; Manthiram, A. Highly flexible, freestanding tandem sulfur cathodes for foldable Li−S batteries with a high areal capacity. *Mater. Horiz.* **2017**, *4*, 249−258.
(61) Chang, C.-H.; Chung, S.-H.; Manthiram, A. Ultra-lightweight PANiNF/MWCNT-functionalized separators with synergistic suppression of polysulfide migration for Li−S batteries with pure sulfur cathodes. *J. Mater. Chem. A* **2015**, *3*, 18829−18834.
(62) Peng, H.-J.; Hou, T.-Z.; Zhang, Q.; Huang, J.-Q.; Cheng, X.-B.; Guo, M.-Q.; Yuan, Z.; He, L.-Y.; Wei, F. Strongly coupled interfaces between a heterogeneous carbon host and a sulfur-containing guest for highly stable lithium-sulfur batteries: mechanistic insight into capacity degradation. *Adv. Mater. Interfaces* **2014**, *1*, 1400227.
(63) Chen, W.; Qian, T.; Xiong, J.; Xu, N.; Liu, X.; Liu, J.; Zhou, J.; Shen, X.; Yang, T.; Chen, Y.; Yan, C. A new type of multifunctional polar binder: toward practical application of high energy lithium sulfur batteries. *Adv. Mater.* **2017**, *29*, 1605160.
(64) Liang, X.; Hart, C.; Pang, Q.; Garsuch, A.; Weiss, T.; Nazar, L. F. A highly efficient polysulfide mediator for lithium-sulfur batteries. *Nat. Commun.* **2015**, *6*, 5682.
(65) Wu, H.; Wu, G.; Ren, Y.; Yang, L.; Wang, L.; Li, X. Co^{2+}/Co^{3+} ratio dependence of electromagnetic wave absorption in hierarchical $NiCo_2O_4$−$CoNiO_2$ hybrids. *J. Mater. Chem. C* **2015**, *3*, 7677−7690.

DOI: 10.1021/acsaem.9b01621
ACS Appl. Energy Mater. 2019, 2, 8153−8162